Copyright Warning

The copyright law of the United States (Title 17, United States Code) governs the making of photocopies or other reproductions of copyrighted material. Under certain conditions specified in the law, libraries and archives are authorized to furnish a photocopy or other reproduction. One of these specified conditions is that the photocopy or reproduction is not to be 'used for any purpose other than private study, scholarship or research.' If a user makes a request for, or later uses, a photocopy or reproduction for purposes in excess of 'fair use,' that user may be liable for copyright infringement. This institution reserves the right to refuse to accept a copying order if, in its judgement, fulfillment of the order would involve violation of copyright law.

ELSEVIER

Contents lists available at ScienceDirect

Chemical Engineering Science

journal homepage: www.elsevier.com/locate/ces



Statistics of particle diffusion subject to oscillatory flow in a porous bed



Jeffrey S. Marshall*, Chloe Arnold, Kelly Curran, Thomas Chivers

Department of Mechanical Engineering, University of Vermont, USA

HIGHLIGHTS

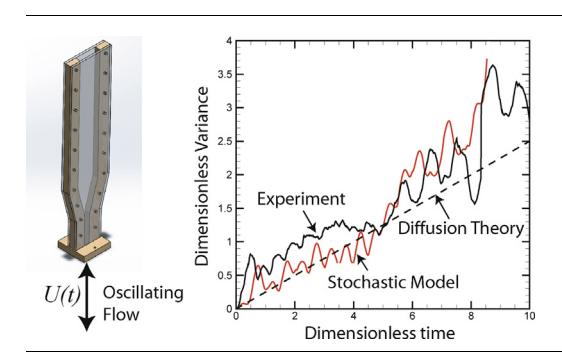
- Oscillating flow enhances particle diffusion in a porous media.
- Diffusion results from oscillation plus random hindering.
- Experiments exhibit statistical measures similar to random walk diffusion.
- Particle hold-up duration exhibits log-normal distribution.
- Stochastic model displays similar characteristics as experiments.

ARTICLE INFO

Article history:
Received 21 August 2020
Received in revised form 12 October 2020
Accepted 20 October 2020
Available online 24 October 2020

Keywords:
Oscillatory diffusion
Porous bed
Particle diffusion
Hindered diffusion

G R A P H I C A L A B S T R A C T



ABSTRACT

An experimental study was conducted of particle diffusion within a porous bed when exposed to oscillatory flow. The particle oscillates up and down within the porous bed in response to the oscillatory flow, but also becomes intermittently stuck for time intervals of varying duration. The combination of oscillating flow and random hindering of the particle motion by the porous bed leads to a diffusive process called oscillatory diffusion. A variety of statistical measures are used to characterize the particle diffusion under the oscillatory flow. These measures show that the experimental data exhibit characteristics of both classical diffusive processes as well as oscillatory processes. The particle hold-up time duration was found to be well fit by a log-normal distribution for all experimental cases examined. A simple stochastic model that captures the key features of the oscillatory diffusion process is shown to yield statistical measures that compare well with experimental data.

© 2020 Elsevier Ltd. All rights reserved.

1. Introduction

Diffusion of particulate matter in a porous medium is important in a number of different applications. This topic is of particular interest for problems involving biological materials, such as tissues, bones, and polymeric films, which at small scales appear as porous networks of connected structures. Drug-encapsulated liposomes and nanoparticles can be used for targeted drug delivery to tissues and tumors. A second application involves delivery of antibiotic chemicals to bacterial colonies within biofilms. Lipo-

E-mail address: jmarsha1@uvm.edu (J.S. Marshall).

somes, nanoparticles and lipid-polymer hybrid nanoparticles, with particle sizes below 100 nm, have been found to be effective for use as carriers (Forier et al., 2014a, 2014b; Li et al., 2015; Cheow et al., 2011; Stewart, 2003; Peulen and Wilkinson, 2011). While a biofilm appears as a gel-like continuum at a large scale, at the scale of a 10–100 nm particle it appears instead as a porous medium formed by a network of connected proteins, called extracellular polymeric substances (EPS). A third application area involves particle diffusion through soil via groundwater transport. This problem is of particular significance in determining the transport of microplastics in the soil, and in estimating the subsequent exposure of soil microbiome to these small plastic particles (da Costa et al., 2019; Hodson et al., 2017; Rillig et al., 2019).

^{*} Corresponding author at: Department of Mechanical Engineering, The University of Vermont, Burlington, VT 05405, USA.

Enhancement of particulate diffusion in a porous medium by acoustic excitation has been demonstrated in several previous experimental studies. For instance, ultrasound has been shown to be effective for directing motion of the nanoparticles onto a specific biological tissue or for triggering liposome bursting and subsequent antibiotic release (Tiukinhoy-Laing et al., 2006; Paul et al., 2014; Schroeder et al., 2009; Huang, 2008). Experiments reported by Ma et al. (2015) found that low-intensity ultrasound significantly enhances transport of liposomes into an alginate gel, including both the liposome transport from solution to the gel outer surface and liposome penetration into the gel. In a follow-up study of diffusion of 20 nm and 100 nm diameter particles in an agarose hydrogel subject to ultrasound, Ma et al. (2018) performed a detailed experimental study that reported significantly enhanced diffusion coefficient in the presence of ultrasound in comparison to the ambient molecular diffusion coefficient. The acoustic excitation was observed in this study to increase the effective diffusion coefficient by between 74 and 133%, depending on the nanoparticle size.

Enhancement of diffusion processes by acoustic excitation in a packed bed of glass spheres was examined by Vogler and Chrysikopoulos (2002) for solute diffusion and by Thomas and Chrysikopoulos (2007) for particle diffusion. The experiments of Thomas and Chrysikopoulos (2007) examined flow through a packed bed of spheres and measured concentration of a tracer particle at the bed outlet versus time. Acoustic excitation was observed to decrease the time required for observation of the concentration peak (i.e., to increase the transport speed of particles through the bed) by about 7%, but not to significantly change the shape of the concentration variation function. Since both acoustic streaming and acoustic radiation pressure would also increase particle advection speed through the bed (Fogler and Lund, 1973), the respective role of diffusion versus these other particle transport mechanisms is not clear.

A one-dimensional stochastic model that attempted to explain enhancement of particle diffusion by acoustic excitation in a porous medium was proposed by Marshall (2016). The model demonstrates that the combination of particle oscillation via an imposed oscillatory flow field (e.g., from the acoustic excitation) and a random hindering of the particle motion (e.g., via interaction of the particles with the porous medium) results in a diffusive process, which is termed oscillatory diffusion. In the limit of many time steps, the stochastic model predictions reduce to a solution of the standard diffusion equation. An expression for the diffusion coefficient in terms of the stochastic model parameters was obtained that leads to excellent agreement between predictions of the stochastic model and the one-dimensional diffusion equation.

The objective of the current paper is to improve fundamental understanding of oscillatory diffusion by examining the detailed motions of individual particles subject to oscillatory flow in a packed bed of spheres. In order to measure diffusion dynamics at the individual particle level, we examined oscillatory motion of small tracer particles in a packed bed of spherical beads using a refractive index-matching immersion in pure glycerin to make the beads transparent. The particles were visually observed to move in an oscillatory manner within the bed, while also becoming intermittently trapped for varying periods of time via a filtration mechanism. Traces of individual particles were ensembleaveraged to obtain statistical measures that describe the problem dynamics. Both traditional statistical measures as well as a new measure developed to highlight the intermittent hindering of the particle motion were examined. The experimental apparatus and method are described in Section 2. The statistical analysis methods used for the experimental data is described in Section 3. The experimental results are presented in Section 4. A stochastic model that captures the essential dynamics of the oscillatory diffusion process is described in Section 5, along with comparison of the stochastic model predictions with experimental data. Conclusions are given in Section 6.

2. Experimental method

Experiments examining particle diffusion in a quasi-twodimensional bed of spheres were conducted using the apparatus shown in Fig. 1. The system used a variable-speed motor to oscillate a piston, causing an oscillatory sloshing flow through the porous bed. Details of the motor-piston assembly are shown in Fig. 1b. The motor shaft rotation frequency (Iron Horse MTR-P50_3BD18) was controlled using an AC drive (Automation Direct GS1-10P5). The shaft frequency was reduced with a worm gear box (Iron Horse WG-175-005-H) with gear ratio of 5. A 10.2 cm pulley on the motor shaft was connected to a similar pulley on a second shaft (the 'bearing shaft', identified as K in Fig. 1b) via a 140 cm V-belt. A crank-and-piston assembly was used to convert the rotational motion of the bearing shaft to vertical motion of the piston. The piston was connected to the rotating bearing shaft via a 19 cm long drive rod (M in Fig. 1b), which was connected to the bearing shaft via an amplitude plate (L in Fig. 1b). The oscillation amplitude was adjusted by moving the connection point of the drive shaft between five available holes drilled into the amplitude plate, which were located at radial distances of 1.3, 2.5, 4.1, 5.8 and 7.4 cm (± 0.1 cm) from the center of rotation of the bearing rod. The drive rod was attached using a ball joint to a vertical 61 cm long threaded piston rod that connected to the piston. The piston was formed from two 1.3 cm PVC end caps and a 1.3 cm coupling, which were sanded to fit inside the 2.5 cm PVC pipe. The threaded piston rod was passed through the piston and was held in place with nuts on each end.

Supports were placed below the system and along the sides to hold the system rigidly in place. A PVC ball valve (D in Fig. 1a) and exit tube were installed to empty the fluid from the system. The 2.5 cm pipe was connected to a 2.5 cm flange (E in Fig. 1a), which was bolted onto the test apparatus. The test apparatus was formed of two polycarbonate sheets with sides formed of oak boards. The test section measured 7.6 cm wide, 1.9 cm thick and 40.6 cm tall, with an additional 10.2 cm long transition section that connects the test section to the flange. The sides of the polycarbonate sheets were coated with 6 mm diameter glass hemispheres. In-between the two layers of hemispheres were placed three layers of borosilicate glass beads with diameter $d_{bead} = 6$ mm. Pure glycerin was used as the working fluid, which was selected in order to match refractive index with the borosilicate glass beads, so that the glass beads were transparent in the glycerin. The glycerin had density $\rho_{gly}=1.26~{\rm g/cm^3}$ and viscosity $\mu_{gly} = 0.95 \text{ Pa} \cdot \text{s.}$

The porosity of the packed bed in the test section was measured by filling the bed with water to a specified height. We then added 300 ml of additional water to the bed and measured the height change Δh of the water in the bed. Dividing the volume of the added water by the channel volume $A\Delta h$, where A is the channel cross-sectional area, yields the bed porosity ϕ . The porosity measurement was repeated 10 times, from which the average and standard deviation were computed to be $\phi=0.334\pm0.006$.

The oscillation amplitude y_{amp} is defined as the amplitude that a passive fluid particle would nominally travel within the porous medium in response to the oscillating motion of the piston. Oscillation amplitude was calibrated by first filling the liquid to a height over the top of the porous bed and measuring the amplitude of oscillation y_{fluid} of the fluid interface under the given piston oscilla-

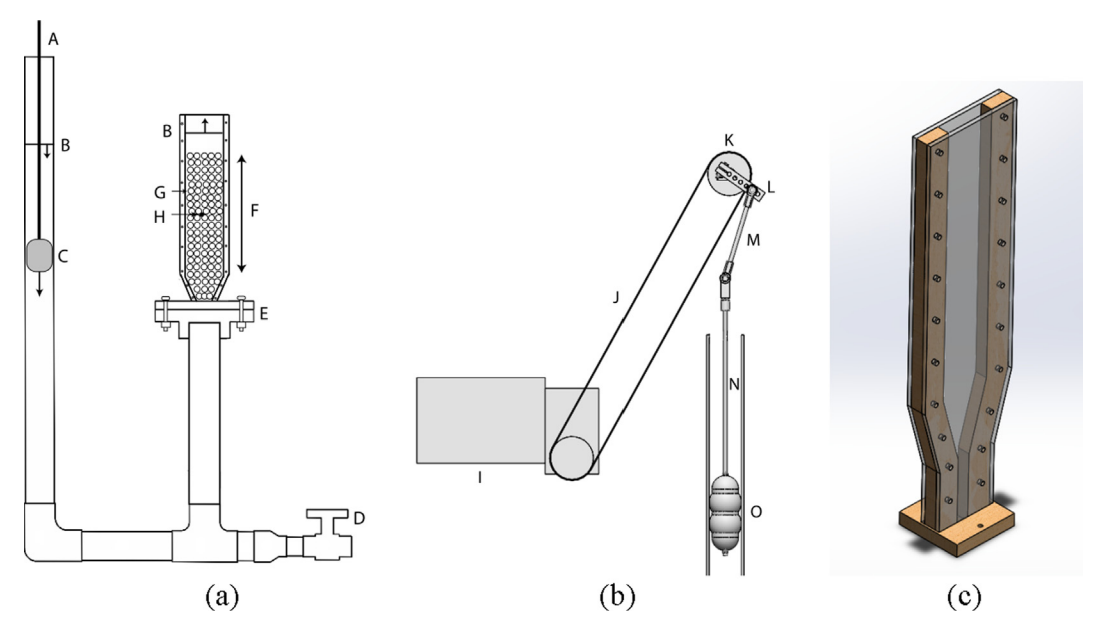


Fig. 1. Schematic diagrams of the experimental apparatus. (a) Overview of apparatus showing [A] piston rod, [B] fluid level, [C] piston, [D] valve, [E] flange, [F] test section, [G] transparent beads, and [H] moving test particle. (b) Close-up of the drive mechanism, showing [I] variable-speed motor, [J] belt, [K] bearings and bearing shaft, [L] bar to set oscillation amplitude, [M] drive shaft, [N] piston shaft, and [O] piston. (c) Close-up of the test section.

tion amplitude and frequency. The nominal oscillation amplitude of a particle within the porous bed is then obtained as

$$y_{amp} = y_{fluid}/\varphi \tag{1}$$

The nominal particle motion within the porous bed (with no particle hindering) is therefore given by the equation

$$y_p(t) = y_{amp}\sin(\omega t) + y_0 \tag{2}$$

where $\omega = 2\pi f_{osc}$ and f_{osc} is the oscillation frequency. The nominal oscillating velocity can be obtained by taking the time derivative of (2), giving

$$v_p(t) = v_{amp}\cos(\omega t) \tag{3}$$

where the amplitude of the velocity oscillation is given by $v_{amp} = \omega y_{amp}$. The parameters y_{amp} , v_{amp} and f_{osc} are used for nondimensionalization of the experimental data.

Each experimental run examined motion in the porous bed of a single moving test particle. The test particle was placed approximately mid-depth in the porous bed at the start of each run using a 25.4 cm long hypodermic needle (14 gauge). Each run was repeated nominally 20 times in order to obtain an ensemble of samples. Two sizes of test particles were used in the experiments. The first particle type consisted of fluorescent red polyethylene spheres (Cospheric) with diameter $d_1 = 0.52 \pm 0.03$ mm, sphericity $\Psi_1 = 0.999996$, and density $\rho_1 = 1.22 \pm 0.03$ g/cm³. The second particle type consisted of black acrylic spheres (Avashop) with diameter $d_2 = 1.3 \pm 0.1$ mm, sphericity $\Psi_2 = 0.996$, and density $\rho_2 = 1.06 \pm 0.02$ g/cm³. None of the test particles were observed to move a measurable amount when suspended in a bath of stationary glycerin. The particle diameter was measured using an optical microscope (Nikon LABOPHOT-2), from which we obtained both the mean and root-mean-square (rms) values for a sample of 25 particles of each type.

The particle density was obtained by measuring the time required for particles to settle a distance of 6 cm at terminal velocity v_T in a beaker of water, which yielded a terminal velocity of 3. 37 ± 0.02 cm/s and 5.10 ± 0.08 cm/s for a sample of 20 particles of type 1 and 2, respectively. The particle density was obtained by an equilibrium condition between drag and gravitational force, giving

$$\rho_p/\rho_w = 1 + \frac{3C_D}{4gd} v_T^2 \tag{4}$$

where for a sphere with Reynolds number $Re_p = \rho_w dv_T/\mu_w$ in the range $Re_p < 800$, the drag coefficient can be approximated using the Schiller-Naumann (1933) correlation as

$$C_D = \frac{24}{Re_n} (1 + 0.15Re_p^{0.687}) \tag{5}$$

The particle Reynolds number at terminal velocity in water was obtained as 19.96 and 74.49 for particles of type 1 and 2, respectively. The uncertainty in the density measurement was estimated from the measured uncertainties in diameter and terminal velocity, δd and δv_T , using the standard variance equation

$$\delta \rho_p = \left[\left(\frac{\partial \rho_p}{\partial d} \right)^2 (\delta d)^2 + \left(\frac{\partial \rho_p}{\partial \nu_T} \right)^2 (\delta \nu_T)^2 \right]^{1/2} \tag{6}$$

The test particles were photographed using a video camera (Sony Handycam) at 30 frames per second, with lighting provided by a 50 W LED flood light. The camera was mounted with viewpoint orthogonal to the side of the polycarbonate sheet on the side of the test section. Fiji particle tracking software, with the plug-in TrackMate, was used to track the motion of the moving particles during each experimental run. This software identifies the test particle at each frame of the video sequence and outputs the location in a coordinate frame. Because we experienced some gaps and errors in the automated particle tracking, we also manually tracked particle paths for each run. The particle location data was used to compute statistical measures of the particle diffusion, as discussed in Section 3.

3. Data analysis

The output of the particle tracking software is a string of data indicating the particle position y(t) at times t_i , i = 1,2,3,4,..., in the vertical direction, denoted by y_i . The statistical measures of a diffusion process change as functions of time. The averages in these statistics are taken over repeated realizations of the process (or different experimental 'runs'). We call each of these runs a *string*, and

refer to the entire set of strings for a given set of parameter values as an *ensemble*. The ensemble average $f_E(t) \equiv \langle f_n(t) \rangle_E$ and the time average $\bar{f}_n \equiv \langle f_n(t) \rangle_T$ of some quantity f(t) are defined by

$$f_{E}(t) = \langle f_{n}(t) \rangle_{E} \equiv \frac{1}{N_{E}} \sum_{n=1}^{N_{E}} f_{n}(t)$$

$$\bar{f}_{n} = \langle f_{n}(t) \rangle_{T} \equiv \frac{1}{T} \int_{0}^{T} f_{n}(t) dt$$
(7)

where subscript n denotes the string number, N_E is the number of strings forming the ensemble, and (0,T) is the time interval over which the data is taken. With this terminology, we define the mean, variance, skew and kurtosis of the particle position as follows:

$$y_{\rm F}(t) = \langle y(t) \rangle_{\rm F} \tag{8a}$$

$$y_{var}(t) = \left\langle \left[y(t) - y_E(t) \right]^2 \right\rangle_E \tag{8b}$$

$$y_{skew}(t) = \left\langle \left[y(t) - y_E(t) \right]^3 \right\rangle_E \tag{8c}$$

$$y_{kurt}(t) = \left\langle \left[y(t) - y_E(t) \right]^4 \right\rangle_F$$
 (8d)

The mean square deviation (MSD) is based on the difference between the measured signal y(t) and a prescribed predicted signal $y_n(t)$, and it is defined by

$$y_{MSD} = \left\langle \left\langle \left[y(t) - y_p(t) \right]^2 \right\rangle_T \right\rangle_F \tag{9}$$

For a normal random walk process the predicted value might be set to the initial particle height y_0 , whereas for oscillatory diffusion the predicted value might be set to an oscillating function of the form (2).

The autocorrelation function $\rho(\tau)$ provides an indication of the correlation between a signal at the current time and the same function at a previous time, hence giving an indication of the degree to which a signal repeats itself. A height difference function $\Delta y(t)$ is defined by

$$\Delta y(t) = y(t) - y_F(t) \tag{10}$$

which is equal to the deviation of the particle height from its ensemble mean value. The autocorrelation function is then defined as

$$\rho(\tau) = \left\langle \left\langle \Delta y(t - \tau) \, \Delta y(t) \right\rangle_T \right\rangle_F \tag{11}$$

where τ is called the lag time.

The power spectrum e(f) describes the spectral make-up of a signal's 'energy' in frequency space. The power spectrum is a plot of the spectral energy density $e(f) = |\hat{y}(f)|^2$ against the frequency f. The power spectrum was computed for each data set, and then averaged over all data sets in the ensemble.

As a baseline, we present examples for these various statistical measures for a random walk process, as is typical of Brownian diffusion. In order to be consistent with the data analysis approach used in our experimental study, we have formed an ensemble with 20 strings and have used a run length with approximately the same number of data points as in the experimental runs. For the example calculation, we selected a case where the diffusion coefficient D and the time step Δt for the random walk calculation were selected as D=0.000125 and $\Delta t=0.01$. The corresponding displacement length ε for each random step was given by

$$\varepsilon = \left[2D\Delta t\right]^{1/2} \cong 0.00158\tag{12}$$

Several different measures for the random walk computations are plotted in Fig. 2, along with theoretical predictions (shown using a dashed line). The ensemble variance $y_{var}(t)$ is plotted versus time in Fig. 2a, and it is found to agree well with the theoretical prediction

$$y_{var}(t) = 2Dt \tag{13}$$

The mean-square deviation (MSD) for the random walk computation was computed as $y_{MSD} = 0.00127$, which compares well with the theoretical value $y_{MSD} = \langle y_{var}(t) \rangle_T \cong 0.00125$. The ratio of the kurtosis to the square of the variance is plotted versus time in Fig. 2b, and it is compared to the theoretical prediction $y_{kurt}(t)/y_{var}^2(t) = 3$ for a normally distributed process.

The autocorrelation $\rho(\tau)$ is plotted as a function of the delay time τ in Fig. 2c. For a random walk process, if a displacement y(t) has a variance given by (13), then the correlation of y(t) with itself at two times s and t is given by

$$E[y(s)y(t)] = 2D\min(s,t) \tag{14}$$

The theoretical value of the autocorrelation function defined by (11) is a linear function of the lag time τ , given by

$$\frac{\rho(\tau)}{y_{var}(T)} = \frac{2D(T-\tau)}{2DT} = 1 - \frac{\tau}{T}$$
 (15)

This theoretical value is shown in Fig. 2c to be in reasonably good agreement with the predicted value from the random walk computation. The computed power spectrum (Fig. 2d) is consistent with the theoretical prediction $e(f) \propto 1/f^2$ for a random walk process, indicated by the dashed line with slope -2 on the log-log plot.

4. Experimental results

The experimental cases listed in Table 1 were analyzed in terms of the statistical measures described in Section 3. Results are given below for Case B-2, which is characteristic of the other cases examined. We then focus more on the measures of particle hold-up for the different cases.

4.1. Standard statistical measures

After the particle is released in the oscillating flow field within the central part of the porous bed, it is observed to oscillate up and down with the imposed oscillatory flow, but to also intermittently pause in a fixed position for different intervals of time before continuing in oscillatory motion. The particle eventually reaches either the upper or lower boundary of the porous bed, at which time the experiment is stopped. A typical particle string y(t) is plotted in Fig. 3, along with the associated velocity v(t). In order to smooth the data in the presence of experimental noise, we computed velocity using a moving least-square fit to a set of five points surrounding the point at which the velocity is desired (Ghazi and Marshall, 2014). The particle position oscillates with the driving frequency, but with an amplitude that varies with time. There are time intervals where the particle oscillation amplitude is very small, and other times where it approaches the nominal amplitude

The mean, variance, and kurtosis of the particle displacement were computed using ensemble averages over the different particle strings (Fig. 4), as discussed in Section 3. These ensemble-averaged measures are found to oscillate in time at approximately the driving frequency due to the phase differences between the dif-

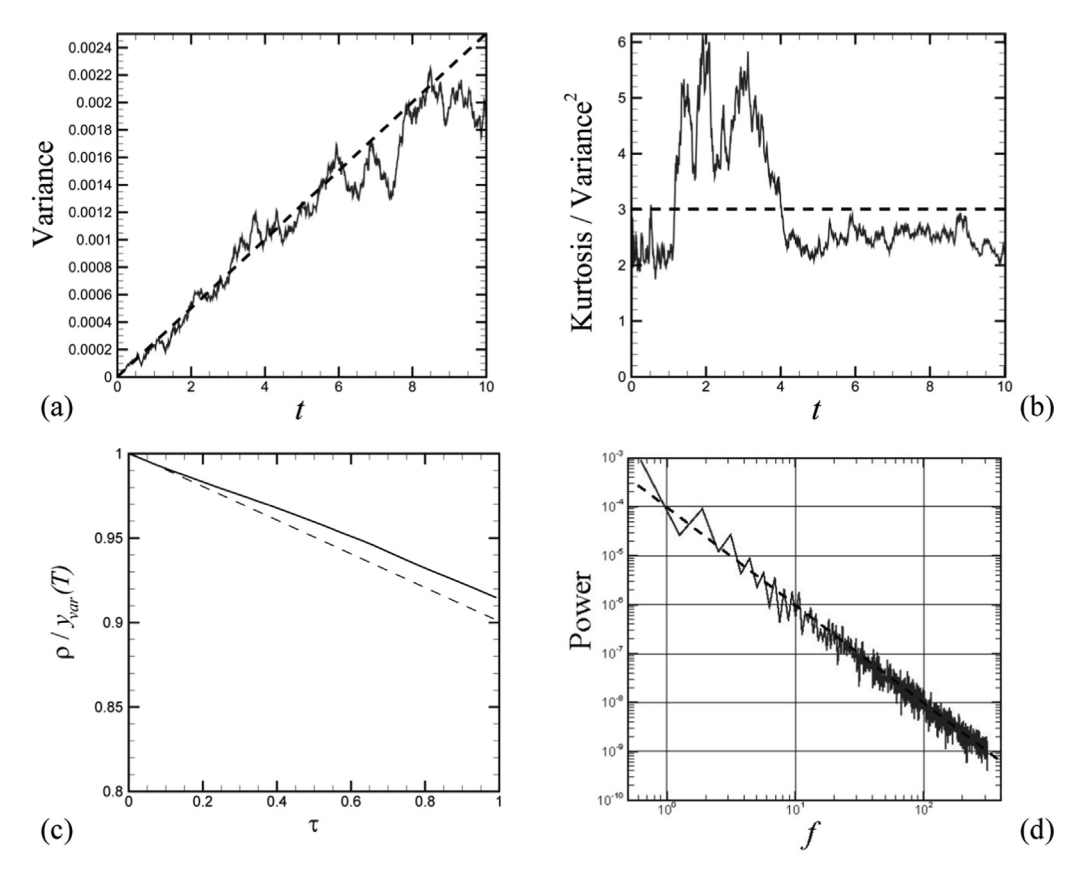


Fig. 2. Plots illustrating statistical measures for a random walk process, showing (a) the ensemble variance and (b) the ratio of the kurtosis over the variance squared as functions of time, (c) autocorrelation as a function of time delay, and (d) the power spectrum. Theoretical predictions are plotted as dashed lines.

Table 1 Parameter values used for the different experimental runs. The uncertainty is ± 1 mm for oscillation amplitude, ± 0.03 mm for diameter of the small particles, and ± 0.1 mm for diameter of the large particles. The uncertainty for frequency is 1% of the recorded value.

Run ID	Test particle diameter d (mm)	Frequency f_{osc} (Hz)	Position amplitude y_{amp} (mm)	Velocity amplitude v_{amp} (mm/s)	Number of repeated runs	Total run time, T/t_{osc}
R-1	0.52	0.15	15.0	14.1	20	260
R-2	0.52	0.25	15.3	24.0	13	138
R-3	0.52	0.50	17.3	54.3	20	1292
R-4	0.52	0.75	12.0	56.5	20	1211
R-5	0.52	0.25	31.0	48.7	21	128
R-6	0.52	0.25	42.9	67.4	20	50
B-1	1.3	0.15	15.0	14.1	21	241
B-2	1.3	0.25	15.3	24.0	20	348
B-3	1.3	0.50	17.3	54.3	20	1846
B-4	1.3	0.75	12.0	56.5	20	3557

ferent particle strings. The effect was observed to diminish as the number of strings increases. The particle mean oscillates in time with a slight upward drift. The variance exhibits a nearly linear increase superimposed on the oscillations, typical of a diffusion process. The ratio of kurtosis to variance squared ranges between 2 and 3, as was also the case for the random walk process (Fig. 2b).

The autocorrelation is plotted in Fig. 5a as a function of the dimensionless lag time $f_{osc}\tau$. It is noted that for a random walk diffusion process, the autocorrelation is a linear function of lag time with decreasing slope, indicated by the dashed line in Fig. 5a. For a purely oscillating process, the signal is perfectly correlated once every oscillation period, and the resulting autocorrelation is an oscillatory function. The curve observed in Fig. 5a for an oscillatory diffusion process is a combination of these two trends, consisting of an oscillating function with a downward trending mean value. The power spectrum plotted in Fig. 5b is found to be similar to that

for random walk processes (Fig. 2d), with a variation closely following a line with slope of -2 on the log-log plot, indicating a $e(f) \propto 1/f^2$ power-law dependence with frequency. A probability density function (P.D.F.) for the velocity is plotted in Fig. 6 which indicates that the particle velocity varies nearly as a Gaussian function (dashed line), with the exception of a high spike at f=0, indicative of a particle that is not moving (or a 'captured' particle).

4.2. Hold-up measures

In an oscillatory diffusion process, particles move periodically up and down in the direction of oscillation, while intermittently getting stuck (captured) for random intervals of time. This behavior is in contrast to the simple one-dimensional random walk process, for which the velocity magnitude is equal to a constant value $v = \varepsilon/\Delta t = [2D/\Delta t]^{1/2}$. Particle hold-up is identified by time steps

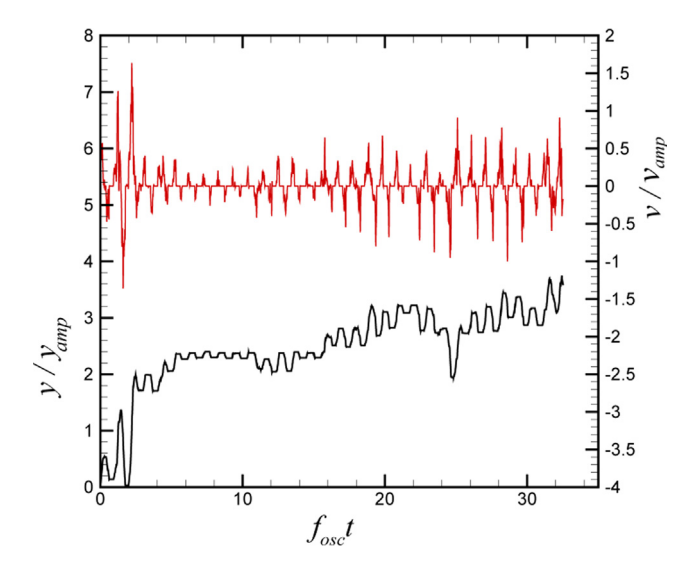


Fig. 3. Plot showing time variation of a sample experimental string for y(t) (bottom, left-hand axis) and v(t) (top, right-hand axis) for Case B-2.

where the absolute value of the particle velocity v is less than a prescribed fraction C_{cut} of the velocity amplitude, or

$$|v| < C_{cut} v_{amp} \tag{16}$$

When (16) is satisfied we say that the particle is in a *captured* state, and when it is not we say that the particle is in a free state. For each hold-up event, the hold-up duration time t_{hold} is set equal to the number of consecutive cycles during which the particle is in a captured state times the time step Δt . The set of hold-up duration times for all strings in an ensemble was sorted into a set of bins, and the number of hold-up events falling in each bin is denoted as $N_{hold,i}$, where the bin number *i* corresponds to a certain interval of the hold-up duration time t_{hold} . A plot showing the values of the normalized number of hold-up events $N_{hold}/(N_{tot}f_{osc}\Delta t_{bin})$ for these bins is given in Fig. 7 for the case B-2, comparing results for C_{cut} values of 0.1, 0.2 and 0.3 for a plot with 50 bins of uniform width. In this plot, N_{tot} is the total number of hold-up events and Δt_{bin} is the bin width. For larger C_{cut} values there are more long-duration hold-up events (with larger values of t_{hold}), whereas for smaller C_{cut} values the long duration hold-up events tend to be broken up into a series of shorter duration events. However, the symbols

in Fig. 7 seem to be scattered about a similar curve for all three cases, suggesting that a common distribution of hold-up events might apply.

In order to characterize the hold-up data, we fit the hold-up distribution plot for each case to a log-normal distribution, with $x \equiv t_{hold} f_{osc}$ treated as a random variable. The fit was done using the following series of steps:

- 1. The experimental hold-up distribution was integrated in x to obtain the cumulative distribution function (C.D.F.), denoted by $F_E(x)$, at the sample points x_i .
- 2. The log-normal C.D.F., denoted by $F_{LN}(x)$, was fit to the experimental C.D.F. using a least-squares fit, where the resulting pair of nonlinear equations was solved for the coefficients μ and σ using the Newton-Raphson iteration method.
- 3. The corresponding log-normal probability density function (P. D.F.) $p_{LN}(x)$ was compared to the experimental P.D.F. for hold-up time, which was obtained by plotting $N_{hold}/(N_{tof} l_{osc} \Delta t_{bin})$ versus x. The bin width Δt_{bin} in this plot was adjusted to eliminate bins with $N_{hold}=0$.

In the above, the log-normal P.D.F. and C.D.F. functions are defined by

$$p_{LN}(x) = \frac{1}{x\sigma\sqrt{2\pi}} \exp\left(-\frac{(\ln x - \mu)^2}{2\sigma^2}\right)$$
 (17a)

$$F_{LN}(x) = \frac{1}{2} + \frac{1}{2} \operatorname{erf}\left(\frac{\ln x - \mu}{\sigma\sqrt{2}}\right)$$
 (17b)

where $erf(\cdot)$ denotes the error function.

An example illustrating these steps is given in Fig. 8 for Case B-4, where for this case and all further cases discussed in this section we use 150 bins, $C_{cut}=0.2$, and a bin width of $f_{osc}\Delta t_{bin}=1$. The lognormal coefficients μ and σ were obtained for each case by a two-step process. In the first step, a square error estimate is defined by

$$E = \sum_{i=1}^{N_{tot}} \left[F_E(x_i) - F_{LN}(x_i) \right]^2$$
 (18)

where $F_E(x)$ is the experimental cumulative distribution function. The value of E is computed over a grid of μ and σ values with step size 0.01, and the values giving the lowest value of E were identified. In the second step, we obtained a formal least-square error

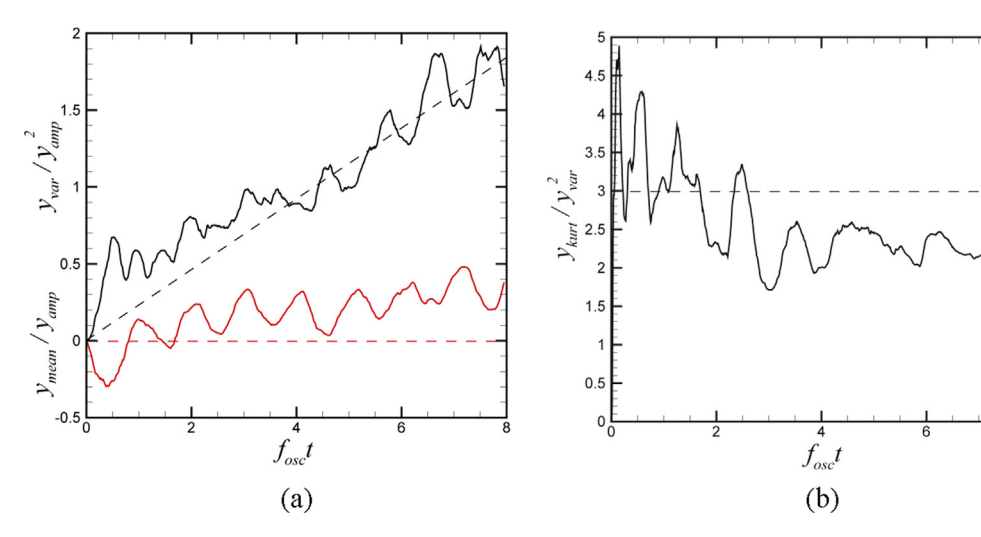


Fig. 4. Plots showing time variation of (a) mean (red) and variance (black) of y position and (b) ratio y_{kurt}/y_{var}^2 for Case B-2. Theoretical results are indicated by dashed lines. (For interpretation of the references to colour in this figure legend, the reader is referred to the web version of this article.)

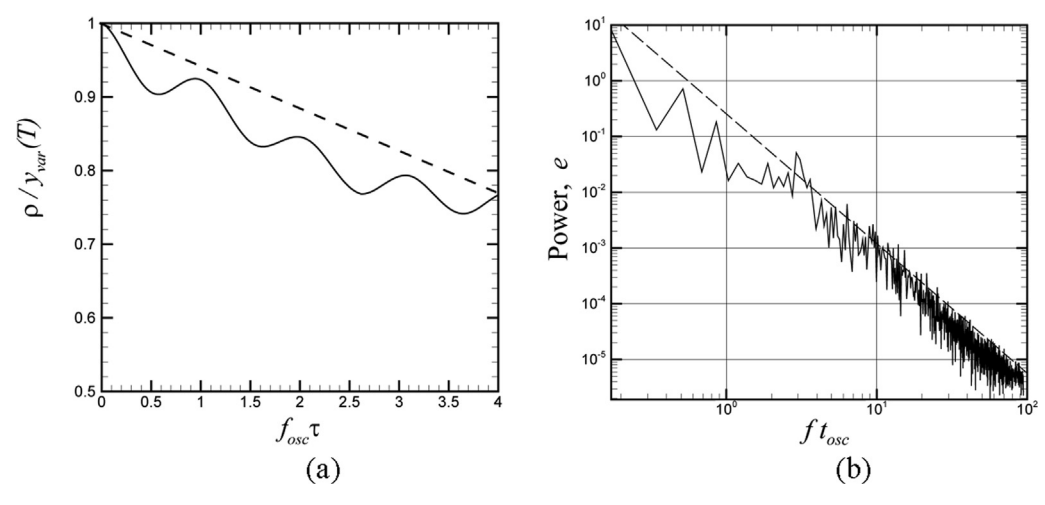


Fig. 5. Plots showing (a) the autocorrelation and (b) the power spectrum for Case B-2. The dashed line in (a) is the theoretical expression in Eq. (15) for a random-walk process, and the dashed line in (b) is for the theoretical power law for random walk diffusion.

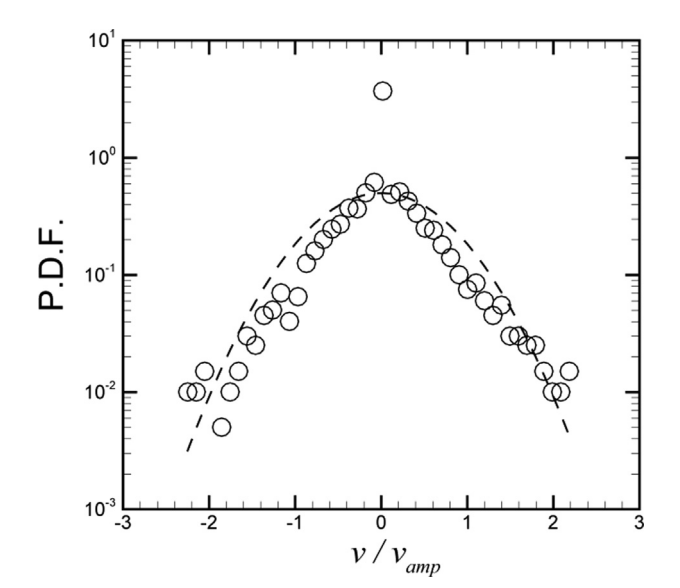


Fig. 6. Probability density function of velocity for Case B-2 at time $f_{\rm osc}t=0.4$. The dashed line is for the Gaussian curve $f(x)=0.5\exp(-x^2)$.

by setting $\partial E/\partial\mu=\partial E/\partial\sigma=0$, and solved the resulting nonlinear system of equations with a Newton-Raphson iteration. The μ and σ values obtained from the first step were used as initial guesses for the iteration. The best-fit values of μ and σ for all cases examined are listed in Table 2.

We note that the criterion for hold-up described above will register a hold-up event for a sinusoidally oscillating velocity field each time the velocity passes through zero. These hold-up events are spurious, however, since the particle is not really captured by the porous media, but rather they are simply an artifact of the oscillating velocity field. In order to eliminate these spurious hold-up events from consideration, we do not include hold-up events with $t_{hold}f_{osc}<0.5$ either in fitting the coefficients μ and σ or in the figures plotting hold-up duration distribution (such as Fig. 8). Consequently, the log-normal function should be viewed as a fit to the longer-time hold-up events, but may not be representative of short-time particle hold-up events. The half-period duration for the hold-up time cut-off used here is based on the length of time that the velocity has a given sign during a single oscillation before changing the direction of motion.

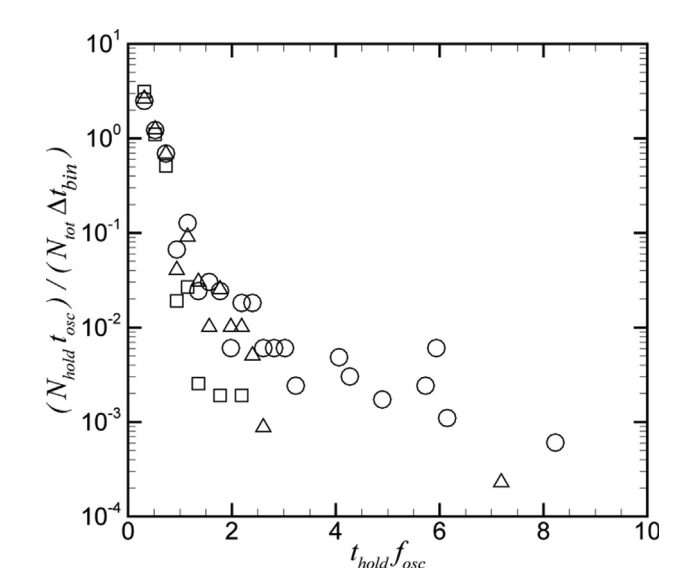


Fig. 7. Plot showing the normalized number of hold-up events as a function of the dimensionless hold time $f_{osc}t_{hold}$ for Case B-2 with different values of the cut-off coefficient: $C_{cut} = 0.1$ (squares), 0.2 (deltas), and 0.3 (circles).

The mean value of the log-normal distribution is given by

$$\bar{x}_{LN} = \exp(\mu + \frac{\sigma^2}{2}) \tag{19}$$

This theoretical mean value for log-normal distributions is found to compare reasonably well with the experimental mean value computed directly from the hold-up time distribution, as listed in Table 2, considering that data for long-time hold-up events is fairly sparse. The total percentage of run time that a particle spends in a free state (with $|v| > v_{cut}$) and in a captured state (with $|v| < v_{cut}$ and $t_{hold}f_{osc} > 0.5$) were computed, as listed in Table 2. The remaining time (not listed in the table) corresponds to time spent by a particle in a captured state with $t_{hold}f_{osc} < 0.5$. For most cases examined, particles were observed to be in a captured state for a very significant percentage of the run time. Also shown in Table 2 is the average frequency of hold-up events, which was computed by the ratio $f_{hold} = N_{tot}/T$ of the total number of hold-up events to the total run time.

The cumulative distribution function depends on the particle diameter d and the oscillation frequency $f_{\rm osc}$ and amplitude y_{amp} .

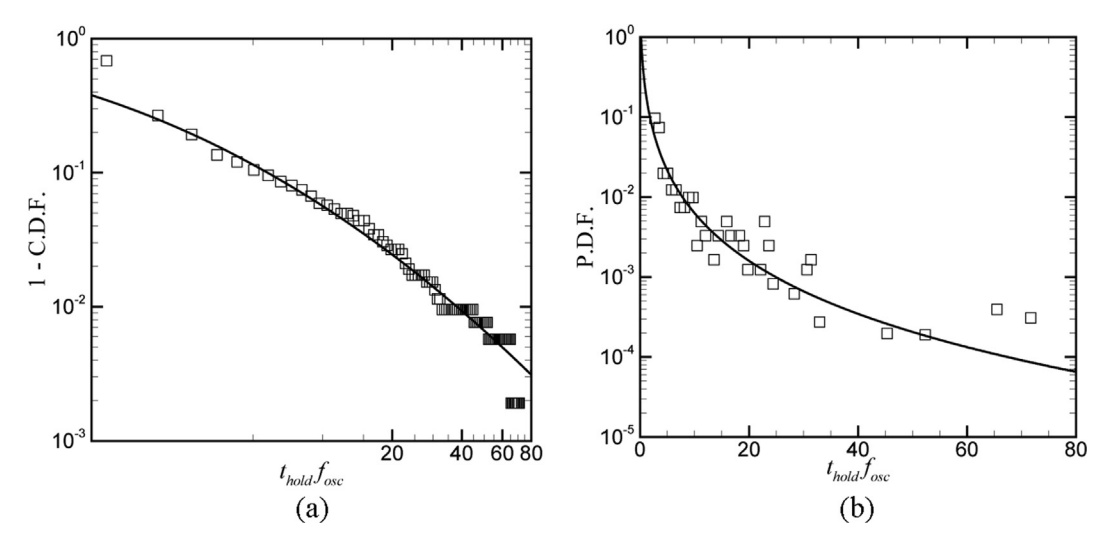


Fig. 8. Example comparing experimental data (symbols) and a log-normal fit (solid line) for (a) the complementary cumulative distribution function (1-C.D.F.) and (b) the probability density function (P.D.F.) for Case B-4.

Table 2Data on frequency of particle hold-up and best-fit values of dimensionless μ and σ coefficients from a log-normal distribution to the cumulative distribution function for particle hold-up time.

Run ID	Log-normal coefficients		Mean hold-up time $t_{hold}f_{osc}$		Percentage time in each state		Hold-up frequency, $f_{hold}t_{osc}$
	μ	σ	Exp.	Log-normal	Free	Capt.	
R-1	-0.125	0.491	0.977	0.996	20.4	47.7	0.489
R-2	-0.121	0.223	0.783	0.908	43.8	9.1	0.116
R-3	0.033	1.314	2.432	2.451	5.1	86.2	0.354
R-4	0.259	1.247	2.691	2.819	5.4	85.0	0.316
R-5	-0.046	0.316	0.935	1.004	14.7	47.3	0.506
R-6	0.044	0.339	1.002	1.107	15.4	46.0	0.459
B-1	-0.387	0.357	0.737	0.724	26.2	17.5	0.237
B-2	-0.086	0.426	0.943	1.005	23.9	23.6	0.250
B-3	-0.392	1.753	3.189	3.141	14.2	56.8	0.178
B-4	-0.557	1.804	2.810	2.916	16.4	41.3	0.147

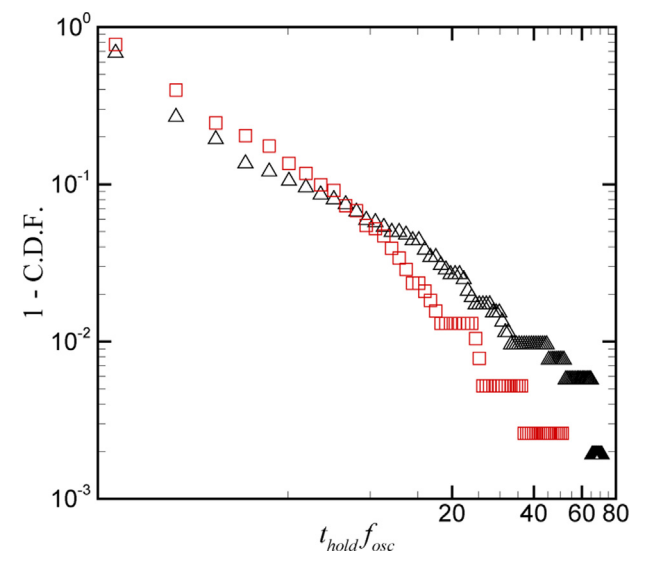


Fig. 9. Comparison of complementary cumulative distribution function for cases with particle diameters of d=0.52 mm (red squares, Case R-4) and d=1.3 mm (black deltas, Case B-4). (For interpretation of the references to colour in this figure legend, the reader is referred to the web version of this article.)

A plot of the complementary cumulative distribution function C.C. D.F. (=1 - C.D.F.) is shown in Fig. 9 for cases with two different particle diameters, $d=0.52\,$ mm (Case R-4) and $d=1.3\,$ mm (Case B-4), with the same oscillation frequency and amplitude. The C.C.D. F. values for both particle sizes are fairly close, with the difference that the larger particles exhibit more long-duration hold-up events and the smaller particles experience more short-duration hold-up events.

A comparison of the effect of oscillation frequency on the complementary cumulative distribution function is shown in Fig. 10a for Cases B-1 through B-4 with frequency varying from $f_{osc} = 0.15 - 0.75$ Hz, all having the same oscillation amplitude and particle diameter. A comparison of the effect of oscillation amplitude on the complementary cumulative distribution function is shown in Fig. 10b for Cases R-2, R-5 and R-6, with amplitude varying from $y_{amp} = 15.3 - 42.9$ mm, all having the same oscillation frequency and particle diameter. Comparing these C.C.D.F. plots with the values of run time listed in Table 1, we see that the experimental runs fall into two categories - cases with relatively short run-time and cases with relatively long run-time. The C.C.D.F. is similar for all cases with short run-time (Cases R-1, R-2, B-1, B-2, R-5, R-6), and it is again similar for all cases with long run-time (Cases R-3, R-4, B-3, B-4); however, the C.C.D.F. for the long run-time cases is shifted significantly to the right of that for the short run-time cases (as soon in Fig. 10a). For cases where the run times were relatively short, the longer-duration hold-up

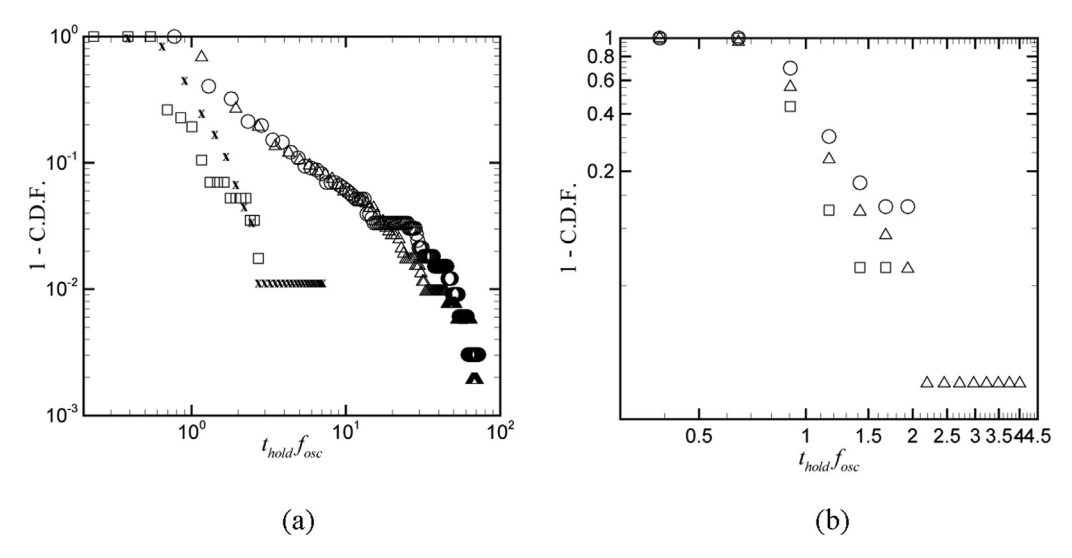


Fig. 10. Comparison of complementary cumulative distribution function for cases with (a) oscillation frequency of $f_{osc} = 0.15$ Hz (squares, Case B-1), $f_{osc} = 0.25$ Hz (X's, Case B-2), $f_{osc} = 0.50$ Hz (circles, Case B-3), and $f_{osc} = 0.75$ Hz (deltas, Case B-4) and (b) oscillation amplitude of $y_{amp} = 15.3$ mm (squares, Case R-2), $y_{amp} = 31.0$ mm (deltas, Case R-5), and $y_{amp} = 42.9$ mm (circles, Case R-6).

events had less of a chance to occur within the experimental time frame than for cases with much longer values of Tf_{osc} , which likely explains the observed difference in the C.C.D.F. plots.

5. Stochastic model

Our proposed mechanism to explain oscillatory diffusion involves the notion that a combination of particle oscillation and random hindering yields a diffusion process (Marshall, 2016). For millimeter-scale particles, the hindering occurs primarily via a filtration process, in which particles randomly enter a pore space that is sufficiently small to temporarily trap the particles. When the velocity direction changes, the particle may or may not be able to escape the pore space.

We propose a simple stochastic model in an effort to illustrate the mechanics of the oscillatory diffusion process. In this model, each particle exists in either a free state or a captured state. The particle relaxation time scale, given by

$$t_{part} = \frac{m}{3\pi\mu_{glv}d} = \frac{\rho d^2}{18\mu_{glv}}$$
 (20)

where $m=(\pi/6)\rho d^3$ is the particle mass, is equal to 1.9×10^{-5} s and 1.1×10^{-4} s for the small and large particle sizes, respectively. Since these values are much smaller than the oscillation time $t_{\rm 0sc}$, which varies from 1.3 to 6.7 s for the different frequencies examined, we can assume that all particles in the free state move within the porous bed in accordance with the fluid velocity given by (3). The pore size b within the porous bed is a random variable that is assumed to exhibit a log-normal distribution, given by

$$b = b_{\min} + \exp(\mu_{pore} + \sigma_{pore} Z) \tag{21}$$

where Z is a random variable with a standard normal distribution and μ_{pore} and σ_{pore} are adjustable parameters. The computations in the current paper were all performed with $\mu_{pore}=0$. The value of b_{\min} is set to the minimum geometrically possible pore size. When a particle moves a multiple of the bead diameter d_{bead} , there is assumed to be a random process during which the particle selects a new pore to enter with size b given by (21). If the particle diameter d < b, then the particle continues to be treated as free, whereas if d > b the particle is considered to be captured by the pore.

A captured particle can be released from the pore when the oscillating velocity field changes sign. However, we observe in our experimental visualizations that sometimes particles bounce around within a pore and remain trapped for multiple cycles. To represent this distribution of release times, we formulated a probabilistic process governing whether or not a captured particle escapes at each time step for which the velocity $v_p(t)$ is opposite in sign to its value at the time of particle capture. At each such time step, a random number p with uniform probability distribution between 0 and 1 is selected. A threshold value t_h is selected in the interval $0 < t_h < 1$, where the value of this threshold is proportional to the product $f_{osc}\Delta t$ so that the resulting particle behavior is independent of the time step size Δt . If $p \leq t_h$, the particle is assigned to be in a free state and moves with velocity given by (3), whereas if $p > t_h$ the particle remains in a captured state and does not move.

This stochastic model was tested for a case with $f_{osc}=0.25$ Hz, $y_{amp}=15.3\,$ mm, and $d=1.3\,$ mm, which is comparable to the experimental Case B-2. The bead diameter was $d_{bead}=6\,$ mm. The minimum pore space is given by the space between three touching beads whose centers form an equilateral triangle, which gives $b_{\min}=(2\sqrt{3}-3)d_{bead}/3\cong0.928\,$ mm. We selected the pore-size parameter $\sigma_{pore}=1\,$ mm and the release threshold $t_h=0.017\,$ for the computations shown as providing reasonable agreement with the experimental data from Case B-2. The stochastic model was used to generate an ensemble of 20 strings with a step size of $\Delta t=0.033\,$ s, from which the statistical measures listed in Section 3 were computed.

A plot showing an example trace data set predicted by the stochastic model for the particle position y(t) and velocity v(t) is shown in Fig. 11. The velocity is observed to be either oscillating sinusoidally (in the free state) or zero (in the captured state). The particle position similarly changes back and forth between oscillating in time (in the free state) and maintaining a constant value (in the captured state). Ensemble-averaged data for the set of 20 data strings are shown in Fig. 12a and b in comparison to the experimental data for Case B-2. In Fig. 12a, the variance is observed to increase in time by fluctuating about a nearly linear increase. A dashed line with the same slope as the linear increase passing through the origin is plotted in Fig. 12a. Fig. 12b shows the ratio of the kurtosis to the square of the variance for y(t), which after an initial transient oscillates about the theoretical value of 3 for a

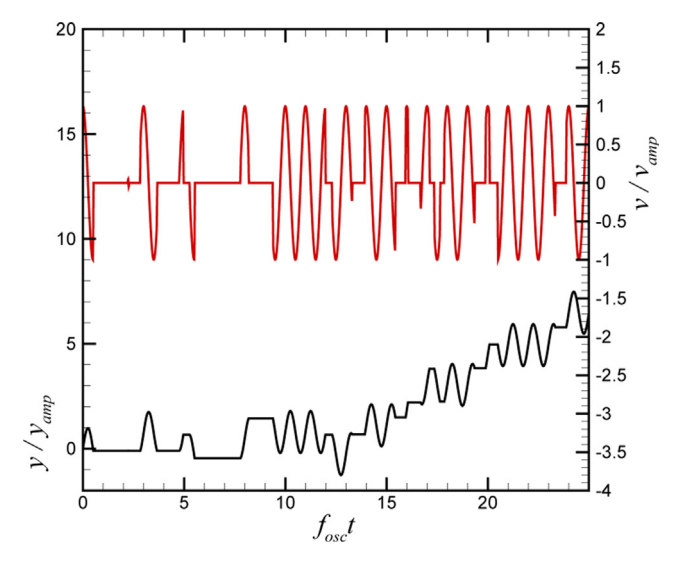


Fig. 11. Plot showing time variation of a sample experimental trace for y(t) (bottom, left-hand axis) and v(t) (top, right-hand axis) for the stochastic model.

normally-distributed process (dashed line). The computed autocorrelation for the stochastic model predictions are plotted against the lag time in Fig. 12c. The predicted autocorrelation curve is nearly straight, as is also the case for a random walk process. The autocorrelation function for the experimental data in Case B-2 exhibited more oscillation than the stochastic model predictions, but both curves are reasonably close to each other. The power spectrum for the stochastic model predictions is plotted in Fig. 12d, with a dashed line representing the $e \propto f^{-2}$ power law on the log–log plot. This power law gives a fairly close fit to the mean slope of the data, as was also the case for the random walk process and the experimental data.

Hold-up data for the stochastic model predictions is sensitive to the value of the threshold parameter t_h . Smaller values of t_h cause the particles to remain captured for longer times, whereas larger values of t_h lead to shorter capture times. In Fig. 13, the complementary cumulative distribution function and the probability density function are plotted for the stochastic model predictions with $t_h=0.017$. The solid lines in these plots represent the best-fit lognormal curves for the experimental data for Case B-2. The stochastic model predictions exhibit more long-duration hold-up events than the experimental log-normal fit. However, even with these differences, the simple probabilistic release model assumed here is nevertheless seen to yield reasonable predictions for distribution of particle hold-up time.

6. Conclusions

An experimental study was conducted of a particle moving under an oscillatory flow field in a porous bed of spherical glass beads. Refractive index matching was used to visualize the particle in the porous bed. The particle is observed to oscillate up and down

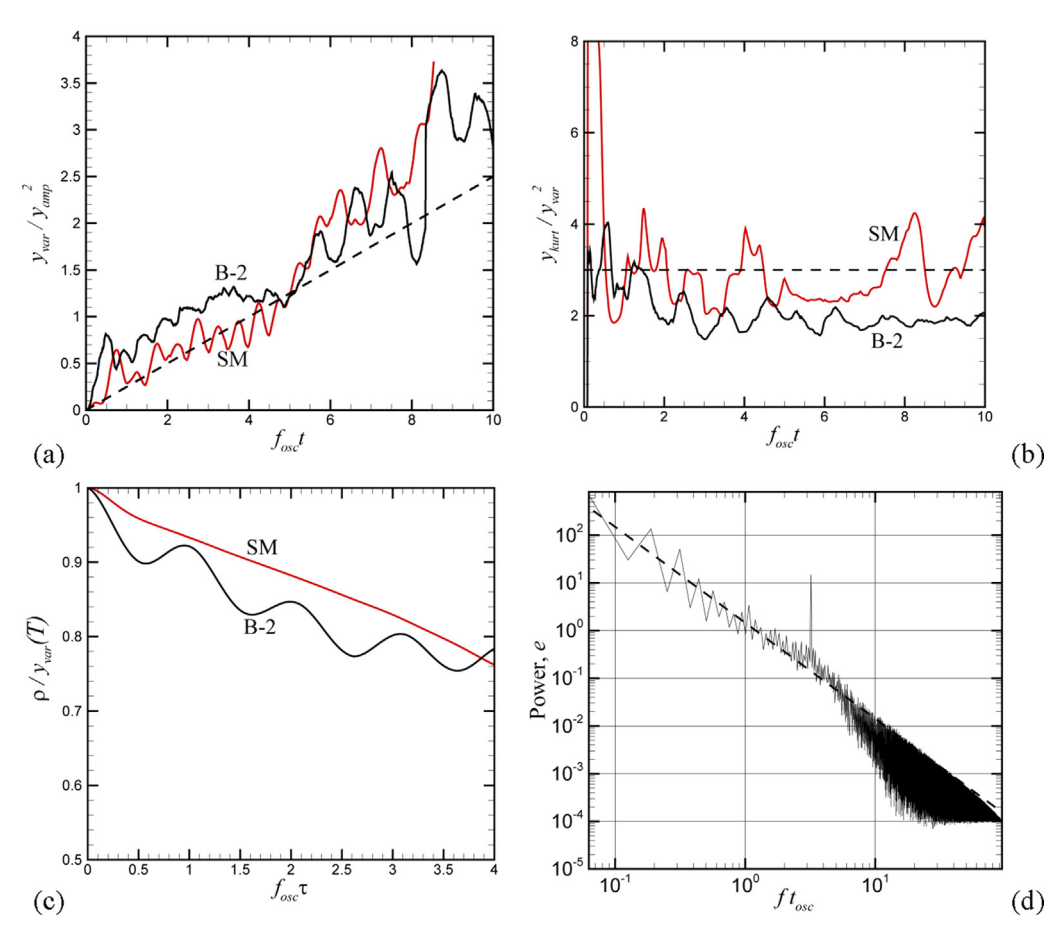


Fig. 12. Plots comparing a variety of statistical measures for the experimental case B-2 (B-2, black line in plots a-c) and the stochastic model (SM, red line in plots a-c): (a) the ensemble variance and (b) the ratio of the kurtosis over the variance squared as functions of time; (c) autocorrelation as a function of time delay, and (d) power spectrum for the stochastic model. Dashed lines indicate (a) best fit to slope of variance passing through origin, (b) theoretical value for a normally distributed process, and (d) f^{-2} power law typical of a random walk process. (For interpretation of the references to colour in this figure legend, the reader is referred to the web version of this article.)

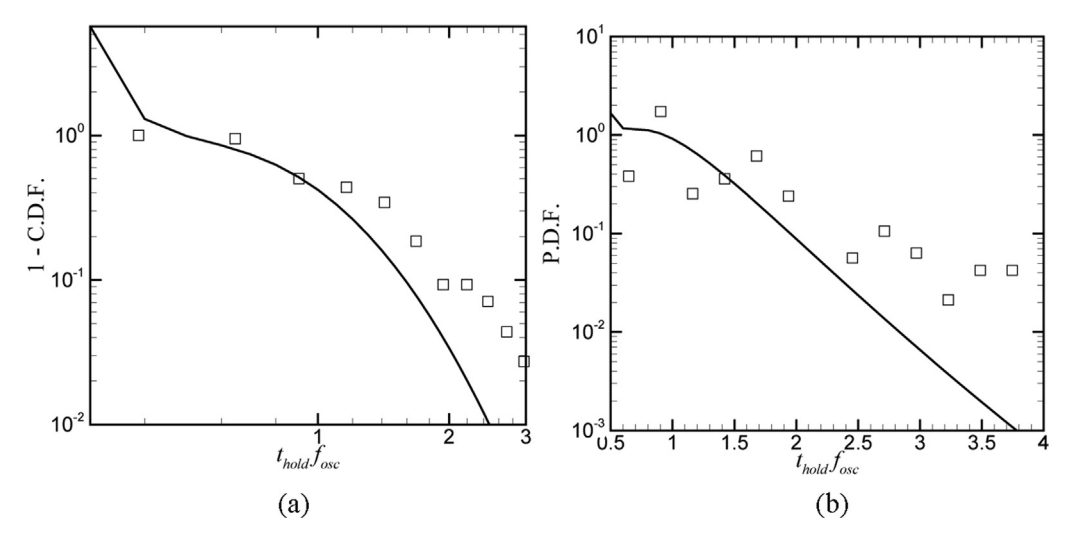


Fig. 13. Plot showing (a) the complementary cumulative distribution function (1-C.D.F.) and (b) the probability density function (P.D.F.), with the stochastic model prediction indicated by symbols and the log-normal fit for the experimental data in Case B-2 indicated by solid lines.

with the imposed oscillatory flow field, but also to intermittently be captured by the porous bed for intervals of various durations. The particle location data was extracted from video images, from which the particle position and velocity were determined as functions of time. Experiments were conducted with two different particle sizes and with various frequencies and amplitudes of the oscillating flow field. Each condition was repeated approximately 20 times to generate an ensemble of data.

A variety of statistical measures were applied to the experimental data for particle position within the porous bed in the presence of oscillatory flow, including ensemble averaging, autocorrelation, spectral analysis, and distribution of particle hold-up times. These measures were found to exhibit many attributes similar to diffusive processes, including nearly linear increase in variance with time, nearly linear decrease in autocorrelation as a function of lag time, and a power-law dependence $e \propto f^{-2}$ between spectral power and frequency. At the same time, the experimental data also exhibited some attributes of an oscillatory process, which resulted in superposition of oscillations for the variance and autocorrelation functions onto the linear dependence typical of diffusive processes. The distribution of particle hold-up duration that characterizes the intermittent particle capturing was found to be well fit by a lognormal distribution. The cumulative distribution plots were used to compare the hold-up distribution data for the different cases examined.

A simple one-dimensional stochastic model was generated to explain the mechanism of the particle diffusion observed in this experiment, which we refer to as oscillatory diffusion. In this model, the particle switches back and forth between a free state and a captured state, with a possibility of a change in state occurring at a set of decision points. The decision points correspond to times when the distance traveled by a particle from its initial position is a multiple of the diameter of one of the beads making up the porous bed. We envision that at each decision point, the particle moves into a new pore within the porous bed. The size of this pore is selected as a random variable with a log-normal distribution, with a minimum value equal to the minimum geometrical value within the bed. If the selected pore size is smaller than the particle diameter, the particle is considered to be captured in the pore; otherwise the particle moves freely. Captured particles are released during times when the velocity direction is reversed depending on whether the value of a random variable exceeds a prescribed threshold. When this stochastic model was applied to the current experiments, the data generated yielded statistical measures that compared reasonably well with those obtained from the experimental data. This agreement lends support to our interpretation of the underlying mechanism of the oscillatory diffusion process.

The current study identified the size ratio between the particle and the glass beads that make up the bed as the key parameter determining the diffusive response of a particle to an imposed oscillatory flow field. We caution, however, that the current experiments and stochastic model are limited to particulate transport at the millimeter size scale, in which particle hold-up is dominated by filtration limitations. For much smaller-scale processes, such as the problem of ultrasound-enhanced diffusion of nanoparticles in a hydrogel, other processes come into play. For instance, for small-scale particles, adhesive capture of the particles by the hydrogel network is as important, or possibly more important, than capture by a filtration process. The stochastic model also assumed that the particle was either moving freely or at rest, and did not account for an in-between state in which the surrounding porous media slows down (but does not stop) the particle motion.

CRediT authorship contribution statement

Jeffrey S. Marshall: Conceptualization, Methodology, Software, Formal analysis, Writing - original draft, Supervision, Project administration, Funding acquisition. **Chloe Arnold:** Methodology, Investigation. **Kelly Curran:** Software, Data curation, Visualization. **Thomas Chivers:** Methodology, Software.

Declaration of Competing Interest

The authors declare that they have no known competing financial interests or personal relationships that could have appeared to influence the work reported in this paper.

Acknowledgements

The authors are grateful for assistance from Xing Jin and Paul Marshall during development of the experimental apparatus, and for conversations with Prof. Jun-ru Wu and Prof. Matthew Wargo regarding this diffusion mechanism. This work was supported by the National Science Foundation under grant number CBET-1926197.

Appendix A. Supplementary material

Supplementary data to this article can be found online at https://doi.org/10.1016/j.ces.2020.116239.

References

- Cheow, W.S., Chang, M.W., Hadinoto, K., 2011. The roles of lipid in anti-biofilm efficacy of lipid-polymer hybrid nanoparticles encapsulating antibiotics. Colloids Surf., A 389, 158–165.
- da Costa, J.P., Paço, A., Santos, P.S.M., Duarte, A.C., Rocha-Santos, C., 2019. Microplastics in soils: assessment, analytics and risks. Environ. Chem. 16, 18–30.
- Fogler, S., Lund, K., 1973. Acoustically augmented diffusional transport. J. Acoust. Soc. Am. 53, 59–64.
- Forier, K., Messiaen, A.S., Raemdonck, K., Nelis, H., De Smedt, S., Demeester, J., Coenye, T., Braeckmans, K., 2014a. Probing the size limit for nanomedicine penetration into *Burkholderia multivorans* and *Pseudomonas aeruginosa* biofilms. J. Control. Release 195, 21–28.
- Forier, K., Raemdonck, K., De Smedt, S.C., Demeester, J., Coenye, T., Braeckmans, K., 2014b. Lipid and polymer nanoparticles for drug delivery to bacterial biofilms. J. Control. Release 190, 607–623.
- Ghazi, C.J., Marshall, J.S., 2014. A CO₂ tracer-gas method for local air leakage detection and characterization. Flow Meas. Instrum. 38, 72–81.
- Hodson, M.E., Duffus-Hodson, C.A., Clark, A., Prendergast-Miller, M.T., Thorpe, K.L., 2017. Plastic bag derived microplastics as a vector for metal exposure in terrestrial invertebrates. Environ. Sci. Technol. 51, 4714–4721.
- Huang, S.L., 2008. Liposomes in ultrasonic drug and gene delivery. Adv. Drug Deliv. Rev. 60, 1167–1176.
- Li, X., Yeh, Y.C., Giri, K., Mout, R., Landis, R.F., Prakash, Y.S., Rotello, V.M., 2015. Control of nanoparticle penetration into biofilms through surface design. Chem. Commun. 51, 282–285.

- Ma, D., Green, A.M., Willsey, G.G., Marshall, J.S., Wargo, M.J., Wu, J.R., 2015. Effects of acoustic streaming from moderate-intensity pulsed ultrasound for enhancing biofilm mitigation effectiveness of drug-loaded liposomes. J. Acoust. Soc. Am. 138 (2), 1043–1051.
- Ma, D., Marshall, J.S., Wu, J.R., 2018. Measurement of ultrasound-enhanced diffusion coefficient of nanoparticles in an agarose hydrogel. J. Acoust. Soc. Am. 144 (6), 3496–3502.
- Marshall, J.S., 2016. A model of ultrasound-enhanced diffusion in a biofilm. J. Acoust. Soc. Am. 139 (6), EL228–EL233.
- Paul, S., Nahire, R., Mallik, S., Sarkar, K., 2014. Encapsulated microbubbles and achogenic liposomes for contrast ultrasound imaging and targeted drug delivery. Comput. Mech. 53, 413–436.
- Peulen, T.O., Wilkinson, K.J., 2011. Diffusion of nanoparticles in a biofilm. Environ. Sci. Technol. 45, 3367–3373.
- Rillig, M.C., de Souza Machado, A.A., Lehmann, A., Klümper, U., 2019. Evolutionary implications of microplastics for soil biota. Environ. Chem. 16, 3–7.
- Schiller, L., Naumann, A., 1933. Über die gundlegenden Berechungen bei der Schwerkraftaufbereitung. Zeitschrift des Vereines Deutscher Ingenieure 77, 318–320.
- Schroeder, A., Kost, J., Barenholz, Y., 2009. Ultrasound, liposomes, and drug delivery: principles for using ultrasound to control the release of drugs from liposomes. Chem. Phys. Lipids 162, 1–16.
- Stewart, P.S., 2003. Diffusion in biofilms. J. Bacteriol. 185 (5), 1485–1491.
- Thomas, J.M., Chrysikopoulos, C.V., 2007. Experimental investigation of acoustically enhanced colloid transport in water-saturated packed columns. J. Colloid Interface Sci. 308, 200–207.
- Tiukinhoy-Laing, S.D., Huang, S., Klegerman, M., Holland, C.K., McPherson, D.D., 2006. Ultrasound-facilitated thrombolysis using tissue-plasminogen activator-loaded echogenic liposomes. Thromb. Res. 119 (7), 777–784.
- Vogler, T., Chrysikopoulos, C.V., 2002. Experimental investigation of acoustically enhanced solute transport in porous media. Geophys. Res. Lett. 29 (15), 1710.